Dispersion Compensation for Huygens' Sources and Far-Zone Transformation in FDTD

Torleif Martin, *Member, IEEE,* and Lars Pettersson, *Member, IEEE*

***Abstract*—The equivalence principle is utilized for generation of both incident plane waves and for near- to far-zone transformation in the finite-difference time-domain (FDTD) method. Small errors will appear due to numerical dispersion when a plane wave is generated by Huygens' sources using an analytical expression for the incident field. These errors can be derived from the numerical dispersion relation in the frequency domain. By using a second-order approximation of the numerical wavenumber it is shown that a simple approximative time-domain compensation procedure for the dispersion can be derived. This has been implemented in a Huygens' source routine and in a time-domain near- to far-zone transformation routine. It is shown that this compensation significantly reduces the errors produced when calculating far-zone scattered fields of low amplitude. It is also shown that it is sufficient to compensate either the Huygens' sources or the time-domain near- to far-zone transformation with respect to dispersion. For validation, plane wave propagation through empty space and scattering of a dipole have been studied.**

***Index Terms*—FDTD methods, numerical dispersion.**

I. Introduction

THE finite-difference time-domain (FDTD) method has been frequently used for antenna and radar cross section (RCS) simulations for over a decade. The method has been popular due to its simplicity and its ability to accurately simulate electromagnetic problems over a wide frequency band. One drawback is numerical dispersion, which, in practice, limits the size of the computational volume. Fields propagating over a large number of grid cells become distorted, which causes errors. This issue has lately received a lot of attention (for example, see [1]–[6]).

In applications where plane wave excitation is used such as scattering calculations, the incident field is applied either on a virtual surface enclosing the object (total field formulation) or as current sources in the object (scattered field formulation). The normal procedure in both cases is to use an analytical expression for the incident field. This analytical expression will not satisfy the finite-difference scheme, which results in a remaining error due to dispersion. One way to partly overcome this problem is to let the plane wave propagate in a one-dimensional (1-D) FDTD grid with the phase velocity adjusted according to the dispersion relation for FDTD and to use a table look-up procedure [5], [6].

In this paper, we introduce a new broad-band method of reducing the dispersion errors by using an approximative time-domain expression for the dispersion. It will also be shown that for scattering simulations, this dispersion compensation can either be applied on the sources for the incident field or in the time-domain near- to far-zone transformation routine, but not necessarily on both simultaneously.

II. Numerical Dispersion Compensation

A plane wave propagating in an FDTD volume will be distorted differently depending on frequency and propagation direction. The amount of distortion can be derived from the dispersion relation [5]

$$\left[\frac{1}{c\Delta t}\sin\left(\frac{\omega\Delta t}{2}\right)\right]^2 = \left[\frac{1}{\Delta x}\sin\left(\frac{\tilde{k}_x\Delta x}{2}\right)\right]^2 + \left[\frac{1}{\Delta y}\sin\left(\frac{\tilde{k}_y\Delta y}{2}\right)\right]^2 + \left[\frac{1}{\Delta z}\sin\left(\frac{\tilde{k}_z\Delta z}{2}\right)\right]^2 \quad (1)$$

where $\tilde{k}_x$, $\tilde{k}_y$, and $\tilde{k}_z$ are vector components of the numerical wave vector $\tilde{\boldsymbol{k}} = \tilde{k}\hat{\boldsymbol{k}}$.

A common way to reduce the influence of dispersion errors for plane wave excitation is to let a plane wave propagate in a 1-D source grid and then apply the result in the three-dimensional (3-D) grid using a table look-up procedure [5]. This method is very accurate for incidence along the x-, y-, or z-axis since the dispersion relation (1) is identical for 1-D and 3-D in this case. For oblique incidence the numerical phase velocity can be adjusted in the 1-D source grid by taking the angular dependence of (1) into account. However, this compensation factor must be calculated at a fixed frequency for example at the center of the incident pulse spectrum. This yields a significant improvement only in a limited bandwidth close to the center frequency.

Below, we will derive a new simple broadband dispersion compensation procedure for arbitrary angles of incidence, although the examples given are mainly for incidence along the z-axis. An approximative expression for the numerical wavenumber was derived in [7] using series expansions for $\sin^2(x)$

$$\tilde{k} = \sqrt{\frac{6}{p^2}\left(1-\sqrt{1-\frac{4}{3}p^2q^2}\right)} + O(q^5) \quad (2)$$

Manuscript received November 20, 1998; revised January 4, 2000.

The authors are with FOA Defence Research Establishment, Linköping, S-581 11 Sweden.

Publisher Item Identifier S 0018-926X(00)03252-X.

where

$$p^2 = s_x^4 \Delta x^2 + s_y^4 \Delta y^2 + s_z^4 \Delta z^2 \tag{3}$$

$$q = \frac{1}{c\Delta t} \sin\left(\frac{\omega \Delta t}{2}\right) \tag{4}$$

and

$$\hat{\boldsymbol{k}} = s_x \hat{\boldsymbol{x}} + s_y \hat{\boldsymbol{y}} + s_z \hat{\boldsymbol{z}} \tag{5}$$

$$\begin{aligned} s_x &= \cos\varphi \sin\theta \\ s_y &= \sin\varphi \sin\theta \\ s_z &= \cos\theta. \end{aligned} \tag{6}$$

This approximative expression for the numerical wavenumber was used in a frequency-domain near- to far-zone transformation in [7]. Below it will be shown that this expression can be further simplified to yield a time-domain operator that approximates the dispersion characteristics of FDTD.

Since $\omega\Delta t \ll 1$ in (4) together with the Courant condition [5] implies that $p^2 q^2 \ll 1$, the expansion

$$\sqrt{1-x^2} \approx 1 - \frac{x^2}{2} - \frac{x^4}{8} \tag{7}$$

can be used in (2) for the innermost square root, yielding

$$\tilde{k} \approx 2q\sqrt{1 + \frac{p^2 q^2}{3}}. \tag{8}$$

Using $\sqrt{1+x^2} \approx 1 + x^2/2$ in (8) gives

$$\tilde{k} = 2q + \frac{p^2 q^3}{3} + O(q^5). \tag{9}$$

Expanding the $\sin(x)$-term in (4) and keeping terms up to x^3 yields

$$q \approx \frac{\omega}{2c} - \frac{\omega^3 \Delta t^2}{48c}. \tag{10}$$

Combining (9) and (10) and neglecting terms higher than ω^3 gives an approximative expression for $\tilde{k}$:

$$\tilde{k} = k_0 + \Delta k \tag{11}$$

where

$$\Delta k = \frac{\omega^3}{24}\left(\frac{p^2}{c^3} - \frac{\Delta t^2}{c}\right) + O(\omega^5) \tag{12}$$

and $k_0 = \omega/c$. Note that p^2 is a function of θ and φ through (3) and (6). Expressions (11) and (12) can be used for reducing the errors in scattering simulations where Huygens' sources are generating the incident field. The compensation procedure can either be applied directly on the Huygens' sources or on the time-domain near- to far-zone transformation routine.

III. Improvement of Huygens' Sources

A. Time-Domain Expression for Dispersion Compensation

When generating a plane wave in FDTD using Huygens' sources [8], an analytical expression is commonly used for the incident field that is created by the current sources on the virtual surface separating the total-field region and the scattered-field region. This wave, however, will be distorted while propagating through the computational volume. Transforming the field into the frequency domain, the plane wave at a distance $\boldsymbol{r}$ from a reference point will propagate according to

$$\boldsymbol{E}(\omega, \boldsymbol{r}) = \boldsymbol{E}_{\text{inc}}(\omega) e^{j\omega t - j\tilde{k}\hat{\boldsymbol{k}}\cdot\boldsymbol{r}} = \boldsymbol{E}_{\text{inc}}(\omega) e^{j\omega t - j(k_0 + \Delta k)\hat{\boldsymbol{k}}\cdot\boldsymbol{r}}. \tag{13}$$

Assuming that $\Delta k \hat{\boldsymbol{k}}\cdot\boldsymbol{r}$ is a small quantity (13) can be written as

$$\boldsymbol{E}(\omega, \boldsymbol{r}) \approx \left(1 - j\Delta k \hat{\boldsymbol{k}}\cdot\boldsymbol{r}\right) \boldsymbol{E}_{\text{inc}}(\omega) e^{j\omega t - jk_0 \hat{\boldsymbol{k}}\cdot\boldsymbol{r}}. \tag{14}$$

Hence, by using (12)

$$\begin{aligned} \boldsymbol{E}(\omega, \boldsymbol{r}) = &\left[1 - j\omega^3 \frac{\hat{\boldsymbol{k}}\cdot\boldsymbol{r}}{24c}\left(\frac{p^2}{c^2} - \Delta t^2\right)\right] \\ &\cdot \boldsymbol{E}_{\text{inc}}(\omega) e^{j\omega t - jk_0 \hat{\boldsymbol{k}}\cdot\boldsymbol{r}} + O(\omega^5). \end{aligned} \tag{15}$$

The $j\omega^3$ part can be converted into a time-domain operator that approximates the dispersion, simply by noting that $(j\omega)^3 \leftrightarrow \partial^3/\partial t^3$. The field in the FDTD grid at a distance $\boldsymbol{r}$ from a reference point can then be written as

$$\begin{aligned} &\boldsymbol{E}(t, \boldsymbol{r}) \\ &\quad \approx \left[1 + \frac{\hat{\boldsymbol{k}}\cdot\boldsymbol{r}}{24c}\left(\frac{p^2}{c^2} - \Delta t^2\right)\frac{\partial^3}{\partial t^3}\right] \boldsymbol{E}_{\text{inc}}\left(t - \frac{\hat{\boldsymbol{k}}\cdot\boldsymbol{r}}{c}\right). \end{aligned} \tag{16}$$

The errors produced when cancelling the incident field at the boundary between the total field-region and scattered field-region can be reduced by using (16) in the source function that is used to excite the equivalent currents on the Huygens' surface. If the incident plane wave is a Gaussian pulse, the corresponding pulse for the Huygens' sources then becomes

$$\begin{aligned} E_{\text{inc}}(t, \boldsymbol{r}) \approx e^{-\alpha(t-T)^2} &\left\{1 + \frac{\hat{\boldsymbol{k}}\cdot\boldsymbol{r}}{24c}\left[\frac{p^2}{c^2} - \Delta t^2\right]\right. \\ &\left. \cdot \left[12\alpha^2(t-T) - 8\alpha^3(t-T)^3\right]\right\} \end{aligned} \tag{17}$$

where

$$T = \frac{\hat{\boldsymbol{k}}\cdot\boldsymbol{r}}{c} + t_0 \tag{18}$$

and t_0 is some initial time delay.

B. Space Limits

Since it is assumed that $\Delta k\hat{\boldsymbol{k}}\cdot\boldsymbol{r}$ is a small quantity, the compensation procedure is only applicable for sizes of the computational volume where the approximation in (14) is valid. An upper limit of $\boldsymbol{r}$ can be estimated for a specific frequency range. Assume that we are interested in wavelengths which correspond to $\lambda > 20\Delta x$ and that $\Delta x = \Delta y = \Delta z$. The largest dispersion errors occur in directions parallel to the Cartesian axes. Therefore, choose $\hat{\boldsymbol{k}} = \hat{\boldsymbol{x}}$ which gives $p^2 = \Delta x^2$ according to (3) and (6). Then, since

$$\omega_{\max} = \frac{2\pi c}{\lambda_{\min}} = \frac{2\pi c}{20\Delta x} \tag{19}$$

$\Delta k_{\max}$ according to (12), becomes

$$\Delta k_{\max} = \frac{\pi^3}{36\,000\Delta x} \tag{20}$$

where it has been assumed that the time-step is close to the 3-D Courant condition so that

$$\Delta t^2 \approx \frac{\Delta x^2}{3c^2}. \tag{21}$$

If we estimate the maximum phase factor $\Delta k\hat{\boldsymbol{k}}\cdot\boldsymbol{r}$ to be $\pi/8$ for which the approximation in (14) is valid, then we can calculate the maximum distance $x = \hat{\boldsymbol{k}}\cdot\boldsymbol{r}$ from the center of the computational volume to the outer Huygens' surface. Using (20) yields

$$x = \frac{\pi}{8\Delta k_{\max}} = \frac{36\,000\Delta x}{8\pi^2} \approx 456\Delta x. \tag{22}$$

This means that it is possible to use the compensation procedure for computational volumes of which the largest dimension is below 900 cells, for a cubic FDTD lattice. Higher order errors will of course still be present, but these are lower at wavelengths longer than $20\Delta x$.

C. Validation for an Empty FDTD Volume

The dispersion compensation procedure for Huygens' sources was validated by letting a plane wave propagate in the z-direction in a computational volume of $60 \times 60 \times 60$ cubic cells ($\Delta x = \Delta y = \Delta z = 0.01$ m). The outer boundary was terminated by a six-cell-thick perfectly matched layer (PML) [9]. A Huygens' surface was positioned ten cells from the outer boundary, which means that the pulse propagated a distance of 40 Δz within the volume. Both a dispersion compensated and an uncompensated Huygens' routine was used. The reference point ($\boldsymbol{r}' = 0$) for the dispersion compensated pulse (17) was chosen to be the center of the computational volume. The pulse width was 20 time steps or $\alpha = 1/(10\Delta t)^2$.

The FDTD calculated electric field one cell above the upper Huygens' surface and one cell below the lower Huygens' surface is shown in Figs. 1 and 2. As seen from the figures, the electric field outside the Huygens' surface is reduced using dispersion compensation. Note that the maximum amplitude in Fig. 1 is nearly a 100 times higher than the maximum amplitude in Fig. 2. This is because the upper Huygens' surface fails to cancel out the pulse that has propagated forward in the z-direction across $40\Delta z$ in the grid, while the error that appears below the lower Huygens' surface is due to the *local* dispersion error between the electric and magnetic field-layers, $\Delta z/2$ apart, at the Huygens' surfaces. This is why there are two pulses in Fig. 2, one for the lower Huygens' surface (closest to the registration point) and one for the upper Huygens' surface.

The shapes of the pulses in Fig. 2 are caused by integration of local errors over the lower and upper surfaces respectively, giving essentially a geometric optics contribution plus delayed edge contributions. These integrated local errors do also occur in the forward direction but since they are much smaller than the cancellation errors discussed above, they cannot be seen in Fig. 1.

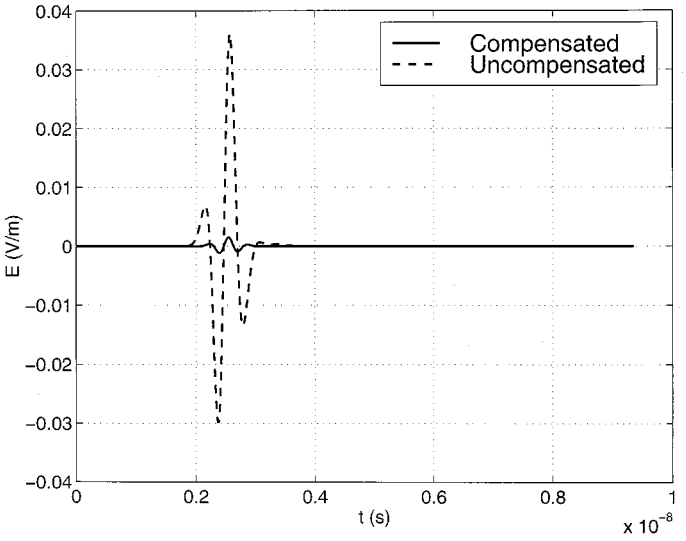

Fig. 1. Electric field outside the Huygens' surface in the forward direction with and without dispersion compensation.

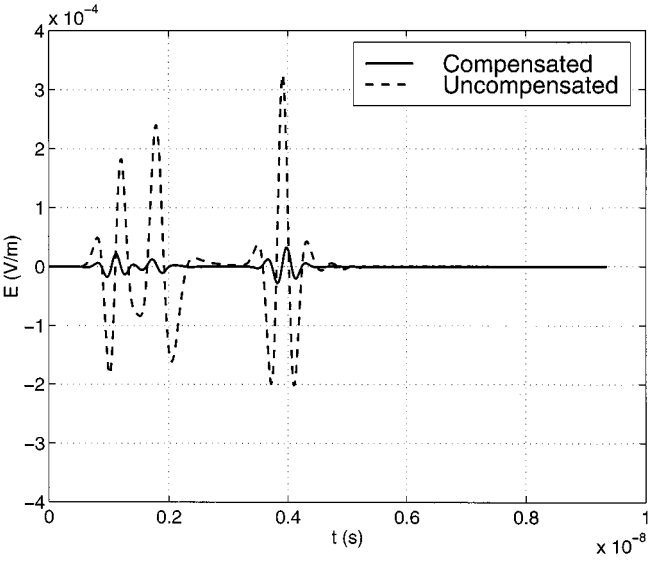

Fig. 2. Electric field outside the Huygens' surface in the backward direction with and without dispersion compensation.

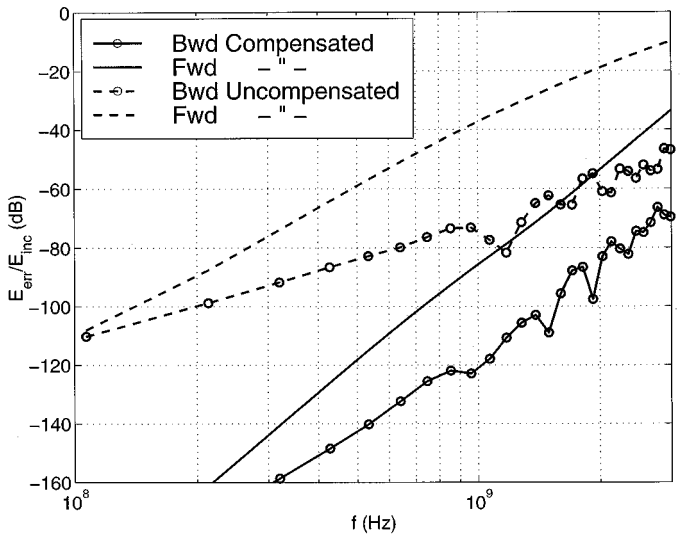

Fig. 3. Frequency-domain response of electric field outside the Huygens' surface in the forward and backward direction with and without dispersion compensation. The electric field is normalized with respect to the incident pulse.

The effects of the dispersion compensation are best illustrated in the frequency domain. The time-domain fields in Figs. 1 and 2 were transformed into the frequency domain and divided with the incident pulse spectrum. The results can be seen in Fig. 3 and as seen from the figure, the level has been reduced by 40 dB at 1.5 GHz ($\lambda = 20\Delta x$). The slope of the curves in the forward direction indicates a change from a ω^3- to a ω^5-dependence in agreement with (12). The slopes for the backward direction indicates a variation with one unit lower exponent; ω^2 and ω^4, respectively, due to the integration effects discussed above.

The incident pulse was computed at each time-step and position on the Huygens' surface during the execution. The total execution time increased by only 3% when using (17) in the Huygens' routine instead of a simple Gaussian pulse. The time difference would be negligible if a table look-up procedure was used.

The procedure above was applied on the Huygens' sources for generation of plane waves in the total-field/scattered-field formulation. It can also be applied in the scattered field formulation where the incident field is applied as sources directly in the scattering material. However, this has not been implemented in this study.

IV. Near- to Far-Zone Transformation

An improved near- to far-zone transformation was proposed in [7], where the spatial shift between the equivalent electric and magnetic currents was preserved. The improved accuracy was illustrated for a frequency-domain near- to far-zone transformation routine. The transform was also further improved by adjusting the phase factor $\exp(jk\hat{\boldsymbol{r}} \cdot \boldsymbol{r}')$ in the Green's function with an approximative numerical wavenumber valid in the FDTD grid.

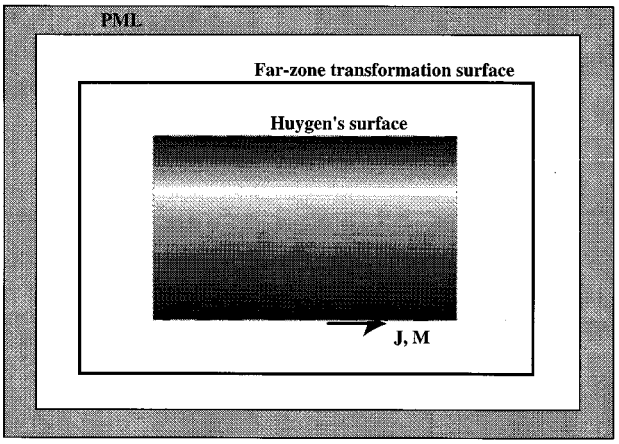

Fig. 4. Far-zone transformation surface outside the Huygens' surface.

In [7], a time-domain version of the near- to far-zone transform without any dispersion compensation was also presented. The resulting vector potentials are

$$\boldsymbol{A}(\boldsymbol{r}, t) = \frac{\mu}{4\pi r} \iint_{S_e} \boldsymbol{J}_s \Big|_{S_h} \left[t - \left(\frac{r - \hat{\boldsymbol{r}} \cdot \boldsymbol{r}'_e}{c} \right) \right] dS' \quad (23)$$

$$\boldsymbol{F}(\boldsymbol{r}, t) = \frac{\varepsilon}{4\pi r} \iint_{S_h} \boldsymbol{M}_s \Big|_{S_e} \left[t - \left(\frac{r - \hat{\boldsymbol{r}} \cdot \boldsymbol{r}'_h}{c} \right) \right] dS' \quad (24)$$

where the lower indexes e and h denote positions in the electric and magnetic grid, respectively, and where

$$\boldsymbol{J}_s = \hat{\boldsymbol{n}} \times \boldsymbol{H}$$
$$\boldsymbol{M}_s = -\hat{\boldsymbol{n}} \times \boldsymbol{E} \quad (25)$$

are the equivalent electric and magnetic surface currents.

Normally when transforming the near-zone fields into the far-zone, the equivalent currents are integrated according to (23) and (24) on a virtual surface in the scattered field region *outside* the Huygens' sources. If the Huygens' sources are applied using an analytical expression for the incident pulse without any dispersion compensation, the remaining dispersion errors will appear as current sources at the Huygens' surface, inside the virtual near- to far-zone transformation surface. This means that they inevitably will contribute to the far-field (see Fig. 4). Applying the compensation procedure for the Huygens' sources, this error will be reduced.

An alternative approach is to apply the compensation procedure in the near- to far-zone transformation routine and perform the transformation on a virtual surface *inside* the Huygens' surface (see Fig. 5). In this case, both the scattered and the incident field will be transformed into the far-zone. The incident field will not contribute to the far-zone in an analytical case. However, the numerical dispersion errors in the FDTD calculated incident field, will yield a net contribution to the far-zone when integrating the vector potentials (23) and (24). If the dispersion compensation is included when calculating the vector

potentials, the errors will be reduced. This can be achieved after first transforming the time-domain vector potentials into the frequency domain. The dispersion compensation can also be combined with a method for improving the time interpolation of the quantized far-zone vector potentials.

A. Time Interpolation

When extracting the field values from FDTD representing the equivalent currents $\boldsymbol{J}_s$ and $\boldsymbol{M}_s$ in (23) and (24), it is necessary to use some type of time interpolation since the relative time-delay generally will not coincide with a multiple of the time-step. This is commonly solved using linear interpolation [10]. We will present a different procedure here which will require some extra storage for the far-zone vector potentials, but that will be more accurate than linear interpolation, when it is combined with a dispersion compensation procedure.

It is exemplified by the vector potential $\boldsymbol{A}$ and the current $\boldsymbol{J}_s$. In practice, the contributions from both the electric and magnetic surface currents will be added simultaneous to a single far-zone storage variable since these are related by

$$\begin{aligned} E_\theta &= -j\omega\left(A_\theta + \eta F_\varphi\right) \\ E_\varphi &= -j\omega\left(A_\varphi - \eta F_\theta\right) \end{aligned} \tag{26}$$

where η is the free-space wave impedance.

The current component $\boldsymbol{J}_s(t-T)$, on the far-zone transformation surface contributes to the far-zone vector potential $\boldsymbol{A}(t)$ according to (23), where T is determined analogous to the time-delay in (18)

$$T = t_0 - \frac{\hat{\boldsymbol{r}}\cdot\boldsymbol{r}'}{c} \tag{27}$$

where

$\hat{\boldsymbol{r}}$: far-zone direction;

$\boldsymbol{r}'$: position vector of the surface current (the subscript c is removed for sake of readability);

$t_0 = r/c$: where r is the distance to the point of observation.

In the far-zone case, the time delay t_0 can be arbitrary as long as T is positive for all $\boldsymbol{r}'$. Let us define a shifted time variable

$$t' = t - T \tag{28}$$

so that $\boldsymbol{J}_s(t') = \boldsymbol{J}_s(t-T)$ (the $\boldsymbol{r}'$-dependence will be omitted in the derivation below for sake of readability). To store the current values at discrete time steps, the time must be quantized according to

$$m = \text{ROUND}\left(\frac{t'}{\Delta t}\right). \tag{29}$$

The stored currents will then be slightly shifted in time where the time shift is

$$\tau = T - m\Delta t. \tag{30}$$

By introducing a new time shifted current variable, $\tilde{\boldsymbol{J}}_s$, we can write

$$\tilde{\boldsymbol{J}}_s(t') = \boldsymbol{J}_s(t - m\Delta t) = \boldsymbol{J}_s(t' + \tau) \tag{31}$$

which represents the current value that is stored in the far-zone array. Transforming (31) into the frequency domain, the relationship between the stored current $\tilde{\boldsymbol{J}}_s$ and the desired current $\boldsymbol{J}_s$ becomes

$$\boldsymbol{J}_s(\omega) = \tilde{\boldsymbol{J}}_s(\omega)e^{-j\omega\tau}. \tag{32}$$

Since $|\tau| \le \Delta t/2$ and, hence, $|\omega\tau| \le 1$, we can expand the exponential function in (32)

$$\boldsymbol{J}_s(\omega) \approx \tilde{\boldsymbol{J}}_s(\omega)\left(1 - j\omega\tau - \frac{\omega^2\tau^2}{2} + j\frac{\omega^3\tau^3}{6} + \frac{\omega^4\tau^4}{24}\right). \tag{33}$$

B. Dispersion Compensation

The dispersion compensation expressed in the frequency domain, can now be added to (33). The time-delay (27) which is dependent on the position vector $\boldsymbol{r}'$, represents a phase factor in the frequency-domain surface integral for the vector potential $\boldsymbol{A}$, i. e.,

$$\boldsymbol{A}(\omega) = \frac{\mu e^{-jkr}}{4\pi r}\iint_S \boldsymbol{J}_s(\omega)e^{jk\hat{\boldsymbol{r}}\cdot\boldsymbol{r}'}. \tag{34}$$

By replacing k in the integrand of (34) with the numerical wavenumber $\tilde{k}$ according to (11), we can define a compensated surface current as

$$\boldsymbol{J}_s^{\text{comp}}(\omega) = \boldsymbol{J}_s(\omega)e^{j\Delta k\hat{\boldsymbol{r}}\cdot\boldsymbol{r}'} \approx \boldsymbol{J}_s(\omega)\left(1 + j\Delta k\hat{\boldsymbol{r}}\cdot\boldsymbol{r}'\right). \tag{35}$$

This dispersion compensated surface current will compensate for the numerical dispersion of the total field if the near- to far-zone transformation is performed in the total-field region. The major impact will be on the incident field which will be cancelled out more effectively, in the same manner as the dispersion compensated Huygens' sources.

Defining a new variable K, from (12) where

$$K = \frac{\Delta k}{\omega^3} = \frac{1}{24}\left(\frac{p^2}{c^3} - \frac{\Delta t^2}{c}\right) + O(\omega^2) \tag{36}$$

and combining (33) and (35), the dispersion compensated surface current can be written as

$$\begin{aligned} &\boldsymbol{J}_s^{\text{comp}}(\omega) \\ &\quad\approx \tilde{\boldsymbol{J}}_s(\omega)\left(1 - j\omega\tau - \frac{\omega^2\tau^2}{2} + j\omega^3\left[\frac{\tau^3}{6} + K\hat{\boldsymbol{r}}\cdot\boldsymbol{r}'\right]\right. \\ &\qquad\left. + \omega^4\left[\frac{\tau}{24} + \tau K\hat{\boldsymbol{r}}\cdot\boldsymbol{r}'\right]\right) \end{aligned} \tag{37}$$

where terms of higher order than ω^4 have been neglected. Equation (37) can easily be transformed into a time-domain filter. However, note that τ is a function of the current position $\boldsymbol{r}'$. For each current component, the filtering requires the time history at five time-steps together with five filter coefficients, uniquely defined at the current positions $\boldsymbol{r}'$. An alternative way is to store each coefficient in front of ω^n in (37), multiply them with the surface current $\boldsymbol{J}_s(t - m\Delta t)$ at each time-step and accumulate

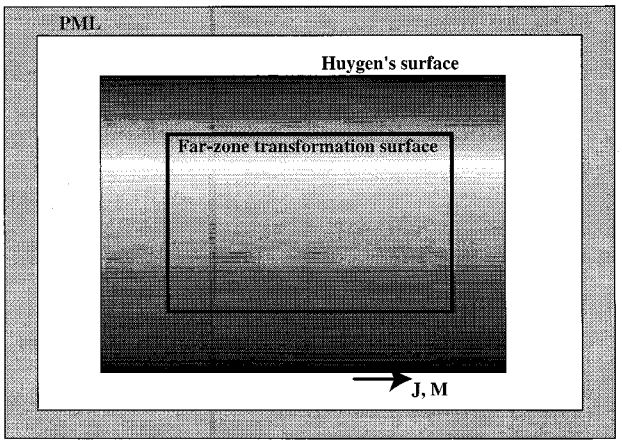

Fig. 5. Far-zone transformation surface inside the Huygens' surface.

the results in five far-zone arrays. The filtering can then be performed after the FDTD execution in the frequency domain, directly on the far-zone arrays after these have been transformed into the frequency domain.

The procedure can be implemented in FDTD as follows: five far-zone arrays are used and the values accumulated in these arrays are symbolically written as

$$\begin{aligned}
\boldsymbol{A}_0(t) &\leftarrow \boldsymbol{J_s}(\boldsymbol{r}', t - m(\boldsymbol{r}')\Delta t)\\
\boldsymbol{A}_1(t) &\leftarrow \boldsymbol{J_s}(\boldsymbol{r}', t - m(\boldsymbol{r}')\Delta t)\,\tau(\boldsymbol{r}')\\
\boldsymbol{A}_2(t) &\leftarrow \boldsymbol{J_s}(\boldsymbol{r}', t - m(\boldsymbol{r}')\Delta t)\,\frac{\tau(\boldsymbol{r}')^2}{2}\\
\boldsymbol{A}_3(t) &\leftarrow \boldsymbol{J_s}(\boldsymbol{r}', t - m(\boldsymbol{r}')\Delta t)\left(\frac{\tau(\boldsymbol{r}')^3}{6} + K\hat{\boldsymbol{r}}\cdot\boldsymbol{r}'\right)\\
\boldsymbol{A}_4(t) &\leftarrow \boldsymbol{J_s}(\boldsymbol{r}', t - m(\boldsymbol{r}')\Delta t)\left(\frac{\tau(\boldsymbol{r}')^4}{24} + \tau(\boldsymbol{r}')K\hat{\boldsymbol{r}}\cdot\boldsymbol{r}'\right)
\end{aligned} \tag{38}$$

where the $\boldsymbol{r}'$-dependence of the different variables has been emphasized. Except for the storage of the time-delay m, this requires only storages for the five $\boldsymbol{r}'$-dependent entities to the right of $\boldsymbol{J_s}$ in (38). After the FDTD execution is finished and the arrays $\boldsymbol{A}_0$–$\boldsymbol{A}_4$ are transformed into the frequency domain, the vector potential is determined by

$$\begin{aligned}
\boldsymbol{A}(\omega) = \boldsymbol{A}_0(\omega) &+ j\omega\boldsymbol{A}_1(\omega) - \omega^2\boldsymbol{A}_2(\omega)\\
&+ j\omega^3\boldsymbol{A}_3(\omega) + \omega^4\boldsymbol{A}_4(\omega).
\end{aligned} \tag{39}$$

Since τ is a small quantity and $\boldsymbol{A}_3$ and $\boldsymbol{A}_4$ are proportional to $\boldsymbol{r}'\cdot\hat{\boldsymbol{r}}$, these two correction terms will dominate over $\boldsymbol{A}_1$ and $\boldsymbol{A}_2$.

C. Validation for an Empty FDTD Volume

The dispersion compensated near- to far-zone transformation was implemented both with and without the dispersion compensation [$K = 0$ in (38)]. A plane wave was incident in the z-direction in an FDTD volume of $60 \times 60 \times 60$ cubic cells. The Huygens' surface was positioned five cells from the PML boundary. The near- to far-zone transformation with the dispersion compensation included, was performed in the total field region ten cells from the PML boundary and five cells inside the Huygens' surface. This corresponds to the situation in Fig. 5. The dispersion compensation was not included in the Huygens' sources. The RCS of the empty volume was calculated at three scattering angles in the E-plane, 0° (forward scattering), 45, and 180°, and the results are presented in Fig. 6.

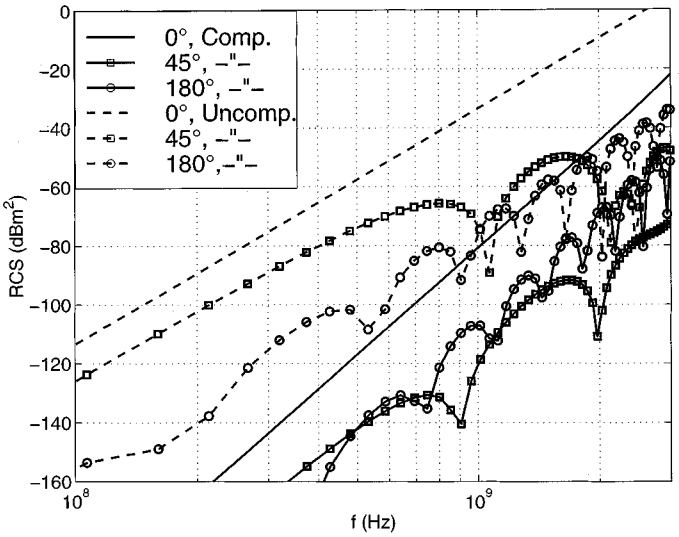

Fig. 6. Radar cross section of an empty FDTD volume. The far-zone transformation is performed in the total-field region. Solid lines shows results with dispersion compensated near- to far-zone transformation routine.

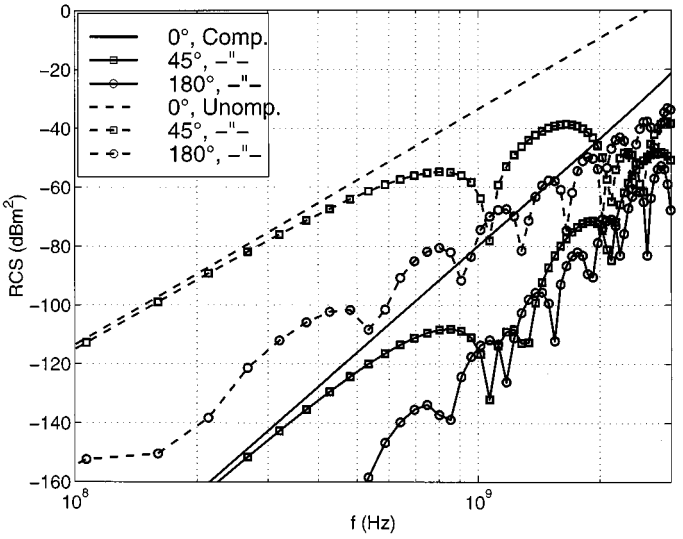

Fig. 7. Radar cross section of an empty FDTD volume. The near- to far-zone transformation is performed in the scattered-field region. Solid lines shows results with dispersion compensated Huygens' routine.

Also, in a second run, the near- to far-zone transformation without dispersion compensation was applied in the scattered-field region, 5 cells outside the dispersion compensated Huygens' surface. The Huygens' surface was positioned 10 cells from the PML boundary in this case. This corresponds to the situation in Fig. 4. The RCS of the empty volume was calculated at the same scattering angles as in previous case and the results are presented in Fig. 7.

As expected, the highest RCS occurs in the forward direction. Note that the RCS levels for the two different approaches

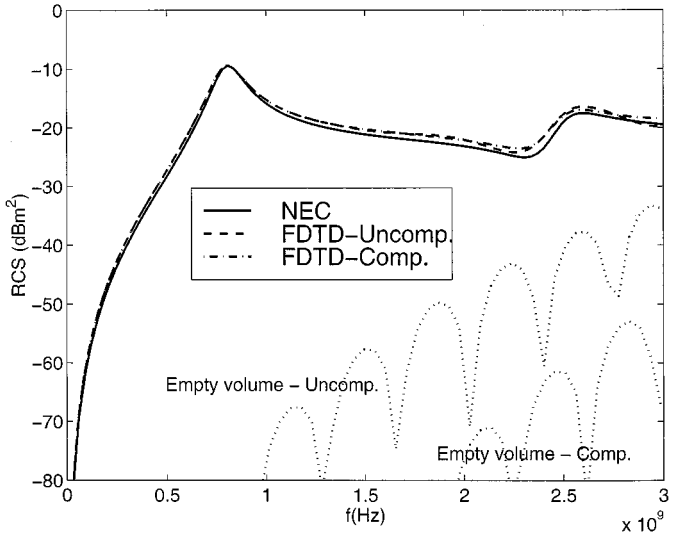

Fig. 8. Monostatic RCS of dipole using MoM and FDTD—with and without a dispersion compensated Huygens' routine. Corresponding FDTD results with the scatterer removed are shown as dotted lines.

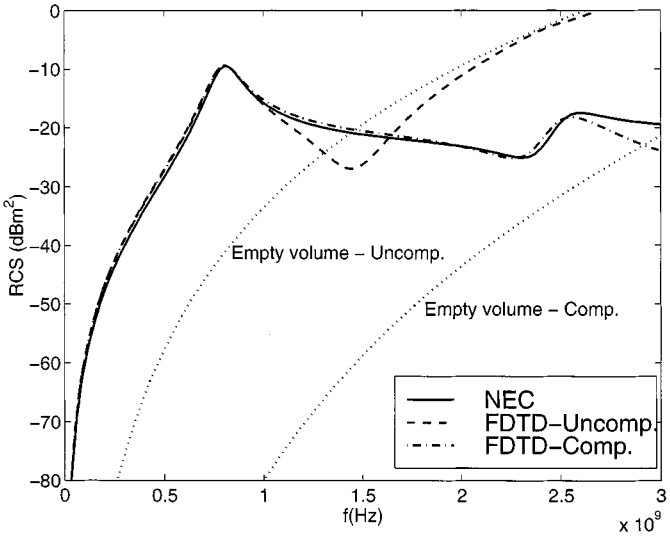

Fig. 9. Bistatic RCS in the forward direction of dipole using MoM and FDTD—with and without a dispersion compensated Huygens' routine. Corresponding FDTD results with the scatterer removed are shown as dotted lines.

are nearly the same. We conclude that either approach is equally good for reduction of dispersion errors of the incident pulse. The RCS levels in Figs. 6 and 7 represent the lower limits of RCS that are possible to simulate for an object for a specific size of the computational volume, a specific incident direction, and at specific scattering directions. Since the RCS can vary much depending on object properties, the importance of the compensation procedure depends on the RCS levels of the object.

The compensation procedure applied on the near- to far-zone transformation can to some extent also reduce the dispersion errors of the scattered field. However, tests on different objects has shown that this effect is generally much smaller than effects on the dispersion errors of the incident pulse. Using only the dispersion compensated Huygens' surface without a dispersion compensated near- to far-zone transformation routine is probably sufficient in most practical situations.

V. Scattering from a Dipole

A resonant dipole was chosen as an example of a scattering object. Obviously the scattered field formulation would be the best choice for this type of problem since no dispersion error would occur for the incident pulse, if normal incidence was considered. However, the dipole is just an example of an object type that has a reasonably low RCS over a large bandwidth just as many other "realistic" objects.

The dipole length was 0.17 m and the radius 1 mm. The RCS of the dipole was calculated using the method of moment (MoM) program NEC-3 and the FDTD method, both with and without dispersion compensation. For FDTD, both compensation procedures described above were used but the results from the two approaches were nearly indistinguishable. Therefore, only the results for the dispersion compensated Huygens' sources are presented in this section.

The size of the computational volume and the cell size were the same as in Section IV ($60 \times 60 \times 60$ cells and 0.01 m, respectively). The near- to far-zone transformation surface was positioned five cells from the PML boundary in the scattered-field region. The Huygens' surface was positioned ten cells from the PML boundary. This means that the distance between the surfaces where dispersion compensation was applied, was 30 cells.

A thin wire model according to [5] was used for the dipole which was oriented in the x-direction. The dipole was modeled using 16 cells, which is the true dipole length adjusted with a half cell size at each end due to the staircasing effects in FDTD. The plane wave was incident in the positive z-direction using a Gaussian pulse. The dipole was modeled using 17 segments in the NEC program.

The monostatic RCS ($\hat{\boldsymbol{r}} = -\hat{\boldsymbol{z}}$) and the bistatic RCS in the forward direction ($\hat{\boldsymbol{r}} = \hat{\boldsymbol{z}}$) were calculated using FDTD with both the uncompensated Huygens' routine and the compensated Huygens' routine. Ideally, due to the symmetry, the results in both directions would be identical.

The monostatic results below 3 GHz (10 cells/λ) can be seen in Fig. 8 and the bistatic results in the forward direction can be seen in Fig. 9. The corresponding results for the empty FDTD volume according to Fig. 7 are also shown as dotted lines for comparison.

In the monostatic case both FDTD solutions follows the NEC solution closely, although the uncompensated FDTD result starts to wiggle at higher frequencies. The RCS levels for the corresponding FDTD volume with the dipole removed are low enough for both cases.

The situation becomes different in the forward direction where the dispersion errors are much higher. As seen in Fig. 9 the uncompensated FDTD result diverges from the NEC-result at 1 GHz (30 cells/λ) while the compensated FDTD result starts to diverge at 2.5 GHz (12 cells/λ). As seen from these results, a margin of approximately 10 dB between the results of the empty FDTD volume and the object is necessary. In this case,

the dispersion compensation makes it possible to simulate RCS values 20 dB lower in the backscattering direction and 30 dB lower in the forward scattering direction.

VI. Conclusion

A time-domain dispersion compensation procedure has been derived and applied on Huygens' sources and in the near- to far-zone transformation routine. The compensation procedure reduces the errors caused by numerical dispersion of the incident pulse in scattering simulations. In most cases, it is sufficient to apply the compensation procedure either at the Huygens' sources or in the near- to far-zone transformation. In the first case the near- to far-zone transformation should be performed outside the Huygens' sources, in the scattered-field region. In the second case, this order should be reversed.

References

[1] P. G. Petropoulos, "Phase error analysis control for FDTD methods of second and fourth order accuracy," *IEEE Trans. Antennas Propagat.*, vol. 42, pp. 859–862, June 1994.

[2] J. Svigelj and R. Mittra, "Grid dispersion error using the nonuniform orthogonal finite-difference—Time domain method," *Microwave Opt. Technol. Lett.*, vol. 10, no. 4, pp. 199–201, Nov. 1995.

[3] J. R. Represa, C. Pereira, M. Panizo, and F. Tadeo, "A simple demonstration of numerical dispersion under FDTD," *IEEE Trans. ED*, vol. 40, pp. 98–102, July 1997.

[4] J. A. Pereda, O. García, A. Vegas, and A. Prieto, "Numerical dispersion and stability analysis of the FDTD technique in lossy dielectrics," *IEEE Microwave Guided Wave Lett.*, vol. 8, pp. 245–247, July 1998.

[5] A. Taflove, *Computational Electrodynamics: The Finite-Difference Time-Domain Method*. Boston, MA: Artech House, 1995.

[6] O. Arikan, U. Oguz, and L. Gurel, "An efficient and accurate technique for the incident-wave excitation in the FDTD method," *IEEE Trans. Microwave Theory Tech.*, vol. 46, no. 6, pp. 869–882, June 1998.

[7] T. Martin, "An improved near- to far-zone transformation for the finite-difference time-domain method," *IEEE Trans. Antennas Propagat.*, vol. 46, pp. 1263–1271, Sept. 1998.

[8] D. E. Merewether, R. Fisher, and F. W. Smith, "On implementing a numeric Huygens' source scheme in a finite difference program to illuminate scattering bodies," *IEEE Trans. Nucl. Sci.*, vol. 27, no. 6, pp. 1829–1833, Dec. 1980.

[9] J.-P. Berenger, "A perfectly matched layer for the absorption of electromagnetic waves," *J. Comput. Phys.*, vol. 114, pp. 185–200, 1994.

[10] R. J. Luebbers, K. S. Kunz, M. Schneider, and F. Hunsberger, "A finite-difference time-domain near zone to far zone transformation," *IEEE Trans. Antennas Propagat.*, vol. 39, pp. 429–433, Apr. 1991.

Torleif Martin (S'96–M'00) was born in Uppsala, Sweden, on December 27, 1962. He received the M.Sc. degree in engineering physics from Uppsala University, Uppsala, Sweden, in 1989, and the Licentiate of Engineering degree in theoretical physics from Linköping Institute of Technology, Sweden, in 1998. He is currently working toward the Ph.D. degree in theoretical physics at the Linköping Institute of Technology, Sweden.

From 1989 to 1995, he was with Saab Military Aircraft, Linköping, Sweden, as a Systems Engineer, dealing mainly with electromagnetic environmental effects. Since 1995 he has been with the FOA Defence Research Establishment, Department of Microwave Technology, Linköping Institute of Technology. His current research interests include computational electromagnetics, in particular, the FDTD method.

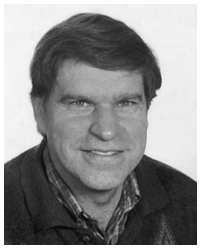

Lars Pettersson (M'81) was born in 1949. He received the M.Sc. and Ph.D. degrees in electrical engineering from Chalmers University of Technology, Göteborg, Sweden, in 1973 and 1979, respectively.

Since 1979, he has been with the FOA Defence Research Establishment, Department of Microwave Technology, Linköping, Sweden. Since 1997 he has been a part-time Adjunct Professor at the Linköping Institute of Technology. His areas of interests are electromagnetics and antennas.